Biomedical Optics EXPRESS

Engineering optically triggered droplets for photoacoustic imaging and therapy

Jacob D. Dove,[1] Paul A. Mountford,[1] Todd W. Murray,[1,2] and Mark A. Borden[1,*]

[1]*Department of Mechanical Engineering, University of Colorado Boulder, 427 UCB, Boulder, Colorado 80309, USA*
[2]*Todd.Murray@colorado.edu*
[*]*Mark.Borden@colorado.edu*

Abstract: Liquid perfluorocarbon (PFC) droplets incorporating optical absorbers can be vaporized through photothermal heating using a pulsed laser source. Here, we report on the effect of droplet core material on the optical fluence required to produce droplet vaporization. We fabricate gold nanoparticle templated microbubbles filled with various PFC gases (C_3F_8, C_4F_{10}, and C_5F_{12}) and apply pressure to condense them into droplets. The core material is found to have a strong effect on the threshold optical fluence, with lower boiling point droplets allowing for vaporization at lower laser fluence. The impact of droplet size on vaporization threshold is discussed, as well as a proposed mechanism for the relatively broad distribution of vaporization thresholds observed within a droplet population with the same core material. We propose that the control of optical vaporization threshold enabled by engineering the droplet core may find application in contrast enhanced photoacoustic imaging and therapy.

©2014 Optical Society of America

OCIS codes: (170.0170) Medical optics and biotechnology; (190.4870) Photothermal effects; (170.5120) Photoacoustic imaging; (160.1435) Biomaterials.

References and links

1. T. O. Matsunaga, P. S. Sheeran, S. Luois, J. E. Streeter, L. B. Mullin, B. Banerjee, and P. A. Dayton, "Phase-change nanoparticles using highly volatile perfluorocarbons: toward a platform for extravascular ultrasound imaging," Theranostics **2**(12), 1185–1198 (2012).
2. N. Rapoport, "Phase-shift, stimuli-responsive perfluorocarbon nanodroplets for drug delivery to cancer," Wiley Interdiscip Rev Nanomed Nanobiotechnol **4**(5), 492–510 (2012).
3. P. S. Sheeran and P. A. Dayton, "Improving the performance of phase-change perfluorocarbon droplets for medical ultrasonography: current progress, challenges, and prospects," Scientifica (Cairo) **2014**, 579684 (2014).
4. O. D. Kripfgans, J. B. Fowlkes, D. L. Miller, O. P. Eldevik, and P. L. Carson, "Acoustic droplet vaporization for therapeutic and diagnostic applications," Ultrasound Med. Biol. **26**(7), 1177–1189 (2000).
5. O. Shpak, M. Verweij, H. J. Vos, N. de Jong, D. Lohse, and M. Versluis, "Acoustic droplet vaporization is initiated by superharmonic focusing," Proc. Natl. Acad. Sci. U.S.A. **111**(5), 1697–1702 (2014).
6. D. S. Li, O. D. Kripfgans, M. L. Fabiilli, J. Brian Fowlkes, and J. L. Bull, "Initial nucleation site formation due to acoustic droplet vaporization," Appl. Phys. Lett. **104**(6), 063703 (2014).
7. A. Hannah, G. Luke, K. Wilson, K. Homan, and S. Emelianov, "Indocyanine green-loaded photoacoustic nanodroplets: dual contrast nanoconstructs for enhanced photoacoustic and ultrasound imaging," ACS Nano **8**(1), 250–259 (2014).
8. A. S. Hannah, D. VanderLaan, Y.-S. Chen, and S. Y. Emelianov, "Photoacoustic and ultrasound imaging using dual contrast perfluorocarbon nanodroplets triggered by laser pulses at 1064 nm," Biomed. Opt. Express **5**(9), 3042–3052 (2014).
9. K. Wilson, K. Homan, and S. Emelianov, "Biomedical photoacoustics beyond thermal expansion using triggered nanodroplet vaporization for contrast-enhanced imaging," Nat. Commun. **3**, 618 (2012).
10. C. W. Wei, J. Xia, M. Lombardo, C. Perez, B. Arnal, K. Larson-Smith, I. Pelivanov, T. Matula, L. Pozzo, and M. O'Donnell, "Laser-induced cavitation in nanoemulsion with gold nanospheres for blood clot disruption: in vitro results," Opt. Lett. **39**(9), 2599–2602 (2014).
11. C. W. Wei, M. Lombardo, K. Larson-Smith, I. Pelivanov, C. Perez, J. Xia, T. Matula, D. Pozzo, and M. O'Donnell, "Nonlinear contrast enhancement in photoacoustic molecular imaging with gold nanosphere encapsulated nanoemulsions," Appl. Phys. Lett. **104**(3), 033701 (2014).

#225025 - $15.00 USD Received 15 Oct 2014; revised 20 Nov 2014; accepted 21 Nov 2014; published 26 Nov 2014

12. J. Jian, C. Liu, Y. Gong, L. Su, B. Zhang, Z. Wang, D. Wang, Y. Zhou, F. Xu, P. Li, Y. Zheng, L. Song, and X. Zhou, "India ink incorporated multifunctional phase-transition nanodroplets for photoacoustic/ultrasound dual-modality imaging and photoacoustic effect based tumor therapy," Theranostics **4**(10), 1026–1038 (2014).
13. E. Strohm, M. Rui, I. Gorelikov, N. Matsuura, and M. Kolios, "Vaporization of perfluorocarbon droplets using optical irradiation," Biomed. Opt. Express **2**(6), 1432–1442 (2011).
14. C. T. Avedisian, "The homogeneous nucleation limits of liquids," J. Phys. Chem. Ref. Data **14**(3), 695–729 (1985).
15. J. E. Shepherd and B. Sturtevant, "Rapid evaporation at the superheat limit," J. Fluid Mech. **121**(-1), 379–402 (1982).
16. H.-Y. Kwak and S. Lee, "Homogeneous bubble nucleation predicted by a molecular interaction model," J. Heat Transfer **113**(3), 714–721 (1991).
17. T. J. Jarvis, M. D. Donohue, and J. L. Katz, "Bubble nucleation mechanisms of liquid droplets superheated in other liquids," J. Colloid Interface Sci. **50**(2), 359–368 (1975).
18. J. G. Eberhart, W. Kremsner, and M. Blander, "Metastability limits of superheated liquids: Bubble nucleation temperatures of hydrocarbons and their mixtures," J. Colloid Interface Sci. **50**(2), 369–378 (1975).
19. F. Caupin and E. Herbert, "Cavitation in water: a review," C. R. Phys. **7**(9-10), 1000–1017 (2006).
20. P. S. Sheeran, V. P. Wong, S. Luois, R. J. McFarland, W. D. Ross, S. Feingold, T. O. Matsunaga, and P. A. Dayton, "Decafluorobutane as a Phase-Change Contrast Agent for Low-Energy Extravascular Ultrasonic Imaging," Ultrasound Med. Biol. **37**(9), 1518–1530 (2011).
21. T. R. C. Thermodynamic Tables, *Non-Hydrocarbons* (College Station, Tex : Thermodynamics Research Center, 1985).
22. J. D. Dove, T. W. Murray, and M. A. Borden, "Enhanced photoacoustic response with plasmonic nanoparticle-templated microbubbles," Soft Matter **9**(32), 7743–7750 (2013).
23. P. A. Mountford, S. R. Sirsi, and M. A. Borden, "Condensation Phase Diagrams for Lipid-Coated Perfluorobutane Microbubbles," Langmuir **30**(21), 6209–6218 (2014).
24. P. S. Sheeran, S. Luois, P. A. Dayton, and T. O. Matsunaga, "Formulation and acoustic studies of a new phase-shift agent for diagnostic and therapeutic ultrasound," Langmuir **27**(17), 10412–10420 (2011).
25. M. F. L'Annunziata, *Handbook of Radioactivity Analysis* (Elsevier, 2012).
26. J. J. Kwan and M. A. Borden, "Microbubble dissolution in a multigas environment," Langmuir **26**(9), 6542–6548 (2010).
27. K. Sarkar, A. Katiyar, and P. Jain, "Growth and dissolution of an encapsulated contrast microbubble: Effects of encapsulation permeability," Ultrasound Med. Biol. **35**(8), 1385–1396 (2009).
28. J. D. Dove, M. A. Borden, and T. W. Murray, "Optically induced resonance of nanoparticle-loaded microbubbles," Opt. Lett. **39**(13), 3732–3735 (2014).
29. H. Goldenberg and C. J. Tranter, "Heat flow in an infinite medium heated by a sphere," Br. J. Appl. Phys. **3**(9), 296–298 (1952).
30. P. G. de Gennes, "Conformations of polymers attached to an interface," Macromolecules **13**(5), 1069–1075 (1980).
31. M. A. Borden, H. Zhang, R. J. Gillies, P. A. Dayton, and K. W. Ferrara, "A stimulus-responsive contrast agent for ultrasound molecular imaging," Biomaterials **29**(5), 597–606 (2008).
32. B. Khlebtsov, V. Zharov, A. Melnikov, V. Tuchin, and N. Khlebtsov, "Optical amplification of photothermal therapy with gold nanoparticles and nanoclusters," Nanotechnology **17**(20), 5167–5179 (2006).
33. A. O. Govorov, W. Zhang, T. Skeini, H. Richardson, J. Lee, and N. A. Kotov, "Gold nanoparticle ensembles as heaters and actuators: melting and collective plasmon resonances," Nanoscale Res. Lett. **1**(1), 84–90 (2006).
34. S. Sirsi, J. Feshitan, J. Kwan, S. Homma, and M. Borden, "Effect of microbubble size on fundamental mode high frequency ultrasound imaging in mice," Ultrasound Med. Biol. **36**(6), 935–948 (2010).
35. J. E. Streeter, R. Gessner, I. Miles, and P. A. Dayton, "Improving sensitivity in ultrasound molecular imaging by tailoring contrast agent size distribution: in vivo studies," Mol. Imaging **9**(2), 87–95 (2010).
36. H. Ju, R. A. Roy, and T. W. Murray, "Gold nanoparticle targeted photoacoustic cavitation for potential deep tissue imaging and therapy," Biomed. Opt. Express **4**(1), 66–76 (2013).
37. P. S. Sheeran, S. H. Luois, L. B. Mullin, T. O. Matsunaga, and P. A. Dayton, "Design of ultrasonically-activatable nanoparticles using low boiling point perfluorocarbons," Biomaterials **33**(11), 3262–3269 (2012).

1. Introduction

Phase change droplets composed of low boiling point perfluorocarbons (PFCs) have received widespread interest from the ultrasound imaging community for diagnostic and molecular imaging applications, and for potential use as therapeutic agents [1,2]. The droplets have long circulation times and can be made small enough to transport outside of the vasculature and interrogate tumors through the enhanced permeability and retention effect [3]. In order to create a therapeutic effect, deliver a drug payload, or provide ultrasound contrast the droplets need to be activated such that the liquid core is converted to a gas that expands to produce a microbubble [4]. Ultrasound has been shown to be effective in triggering acoustic droplet

#225025 - $15.00 USD Received 15 Oct 2014; revised 20 Nov 2014; accepted 21 Nov 2014; published 26 Nov 2014
(C) 2014 OSA

vaporization, with the peak negative pressure created within the droplet sufficient to produce the phase transformation. While the mechanism for creating a cavitation nucleus with a droplet of a given size is not entirely clear, super-harmonic focusing of ultrasound waves within droplets has been determined to play a role in acoustic droplet vaporization at experimentally measured ultrasound pressures [5,6].

More recently, phase change agents have been proposed as promising photoacoustic contrast agents [7–13]. In this case, PFC droplets are designed to absorb light at the wavelength of interest by incorporating a light absorbing species within the droplet or on the periphery. Optical absorption of pulsed laser light creates a local temperature rise within the droplet through the photothermal effect and produces high frequency pressure waves. Under sufficiently high laser fluence, a phase transition is induced; a process termed optical droplet vaporization (ODV). ODV based contrast agents have several advantages over photoacoustic contrast agents that rely solely on photothermal heating to produce acoustic waves in that a) the vaporization event produces an exceptionally strong photoacoustic response, exceeding that from the thermoelastic expansion and allowing for improved photoacoustic imaging contrast, b) the microbubbles created through ODV can provide ultrasound contrast in dual mode imaging scenarios and c) the light absorbing species incorporated into the droplets remain after vaporization and can be used to provide lasting enhanced photoacoustic contrast [7–9]. There has been progress towards modifying the optical absorbing structure within the droplet core in order to maximize the temperature rise and thus lower the optical fluence required to produce ODV [8,11]. In addition, ODV in the near-infrared (NIR) region of the spectrum, where the optical penetration within tissue is large, has been demonstrated by incorporating NIR absorbing gold nanorods into the droplet core or clustered gold nanospheres on the droplet surface [8–10].

It has long been known that heterogeneous nucleation can be suppressed by immersing a volatile liquid, in the form of a droplet, in another nonvolatile liquid in which it has low solubility [14,15]. The liquid-liquid interface is free of solid motes and gas pockets, thus inhibiting the nucleation process and, in the case of heated droplets, leading to a superheated liquid core in a metastable state. With sufficient heating, homogeneous nucleation may occur at a temperature that is approximately 90% of the critical temperature for many substances [14–19], where the critical temperature is the maximum temperature for which the liquid is in a thermodynamically stable state. It is also noted that for very small droplets, surface tension at the liquid-liquid interface can lead to a substantial increase in the pressure in the droplet core required to maintain mechanical equilibrium and further hinder bubble nucleation [20]. When large superheats occur, it can lead to explosive vaporization events once bubble nucleation is triggered, which in turn can produce a large acoustic response and potentially induce therapeutic effects in tissue.

The droplet core material is arguably the most critical parameter to consider in the development of PFC droplets that can be triggered using a laser source at depth in biological tissue (without exceeding laser safety guidelines). In this paper, we study the effect of droplet core material on the ODV threshold with an aim towards reducing the threshold laser fluence at which ODV can be achieved. Nanoparticle-templated microbubbles with different gas cores were subjected to high pressures to induce condensation; producing nanoparticle-templated droplets. The microbubble condensation approach allowed for droplets to be produced of volatile PFCs with equilibrium boiling temperatures below room temperature, but which remain in a metastable liquid state above room temperature. The core material is found to have a profound effect on ODV, with more volatile PFC droplets vaporizing at a lower laser fluence. The effects of droplet size on vaporization threshold are discussed, as well as a proposed mechanism for the relatively broad distribution of vaporization thresholds observed within a droplet population with the same core material.

#225025 - $15.00 USD Received 15 Oct 2014; revised 20 Nov 2014; accepted 21 Nov 2014; published 26 Nov 2014
(C) 2014 OSA

2. Materials and methods

2.1 Microbubble fabrication

Microbubbles were fabricated with 1,2-diarachidoyl-*sn*-glycero-3-phosphocholine (DAPC), 1,2-distearoyl-sn-glycero-3-phosphorethanolamine-N-[methoxy (polyethylene glycol) 2000] (DSPE-PEG2K), and 1,2-distearoyl-sn-glycero-3-phospho-ethanolamine-N [biotinyl (polyethylene glycol)-2000] (DSPE-PEG2K-B) purchased from Avanti Polar Lipids (Alabaster, AL, USA). Three different PFC gas cores were used during fabrication: octafluoropropane (C_3F_8), decafluorobutane (C_4F_{10}) and dodecafluoropentane (C_5F_{12}) purchased from FlourMed (Round Rock, TX, USA) at 99% wt. purity. The boiling temperatures at ambient pressure are −36.7 °C for C_3F_8, −1.96 °C for C_4F_{10} and 29.24 °C for C_5F_{12} [21].

The sonication method was used to fabricate bubbles with gas cores of C_3F_8 and C_4F_{10}. First a lipid solution containing DSPE-PEG2K-B, DSPE-PEG2K, and DAPC at molar ratios of 1:9:90 was heated above the phase transition temperature of DAPC (66° C) to promote lipid mixing. The lipid solution was then cooled to room temperature and sonicated with a Branson 450 Sonifier (Branson, Dandurt, CT) on low power (2/10) with the tip submersed in the solution for 30 seconds to ensure the lipids were fully dispersed. The sonicator tip was moved to the gas-liquid interface and the headspace was flooded with C_3F_8 or C_4F_{10} for 10 seconds. The interface was then sonicated at full power (10/10) for 10 seconds, creating a bubbly mixture. Microbubbles were extracted with a syringe and washed three times at 100 RCF for 1 minute with a centrifuge (Eppendorf 5804 Centrifuge, Hauppauge, NY, USA) to concentrate bubbles with diameter of 4 μm and greater. The supernatant was collected and stored for nanoparticle conjugation.

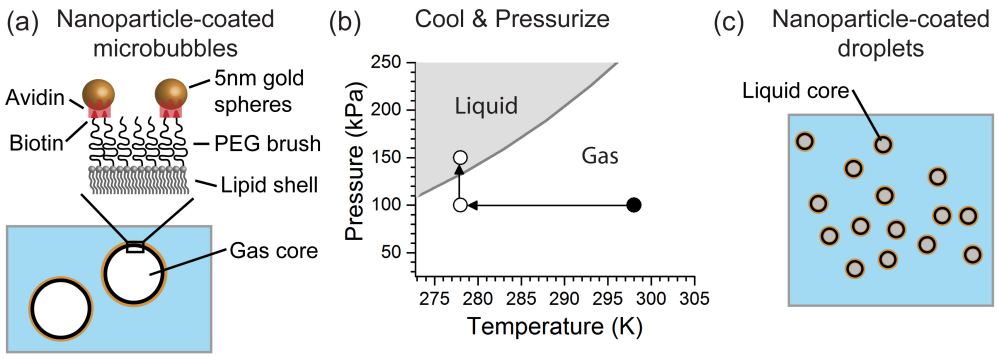

Fig. 1. Fabrication procedure to produce nanoparticle-loaded microbubble condensed droplets. (a) Nanoparticle-loaded microbubbles are (b) cooled and pressurized to create (c) optically active droplets.

Microbubbles with a C_5F_{12} core were made using amalgamation. C_5F_{12} is a liquid at room temperature and C_5F_{12} gas was produced by heating 100 mL of liquid C_5F_{12} to 50 °C in an air tight container on a hot plate. The headspace was removed by vacuum and gaseous C_5F_{12} was allowed to fill the headspace. The lipid solution was prepared in a similar fashion and identical mole fractions as described above. However, 2 mL of the heated lipid solution was extracted, placed in a 3 mL vial, and capped creating an air-tight seal. The headspace of the 3 mL vial was removed via vacuum and refilled with C_5F_{12} gas. The gas exchange process was repeated 3 times. The vial was amalgamated for 45 seconds producing a bubbly mixture. The bubbles were extracted with a syringe and removed from the 50° C environment for washing at 100 RCF for 1 minute to concentrate bubbles with diameter of 4 μm and greater. The supernatant was collected and placed in the heated environment for nanoparticle conjugation.

#225025 - $15.00 USD Received 15 Oct 2014; revised 20 Nov 2014; accepted 21 Nov 2014; published 26 Nov 2014
(C) 2014 OSA

Nanoparticles were attached to the microbubble shell following a previously described avidin-biotin conjugation scheme [22]. First, the bubbles were sized to estimate the number of binding sites. Gold spheres, 5 nm in diameter with one avidin molecule per nanoparticle, were purchased from Nanopartz (Loveland, CO, USA). The nanoparticles were added to the bubble mixture at a 1:1, nanoparticle:biotin (avidin:biotin) ratio. The nanoparticle and microbubble mixture was continuously mixed with an end-over-end rotator for 2 hours. Note that the bubbles with a gas core of C_5F_{12} were mixed at an elevated temperature of 50° C. After 2 hours, the nanoparticle-coated microbubbles were allowed to separate from the unconjugated nanoparticles through gravitational floatation, producing nanoparticle-templated microbubbles as depicted in Fig. 1(a)

2.2 Condensation of nanoparticle-coated microbubbles

Droplets were fabricated following the condensation procedure previously described in the literature [20,32]. In brief, a two-step process (Fig. 1(b)) was used to condense the microbubbles. First the nanoparticle-loaded microbubbles were placed in a syringe and cooled down in an ice bath for 30 seconds. This process lowers the required pressure for condensation. Second, a manual step in pressure (~50 psi) was applied to the syringe. The increase in pressure caused the microbubbles to condense, producing droplets with a liquid core. Before the application of pressure, the bubble mixture was pink and opaque. After pressurizing, the bubbles condensed and the mixture became transparent while remaining pink in color.

2.3 Droplet characterization

Microbubbles were sized via electro-impedance volumetric zone sensing using a Beckman-Coulter Multisizer III. The aperture tube was 30 μm in diameter. The microbubbles were diluted in 10 mL of Isoton and measured to produce a size distribution. This was repeated three times and the size distributions were averaged.

The size distribution of the microbubble condensed droplets was measured by dynamic light scattering with a Malvern Nano-S90 (Worcestershire, UK). The refractive index for liquid C_4F_{10} was assumed to be 1.276 and the surrounding water was 1.348 [25]. The nanoparticle-loaded droplets were diluted in water and placed in a micro-cuvette (Zen 2112, Mavern, Worcestehshire, UK) with a total volume of 12 μL for sizing. This process was repeated 3 times and the size distributions were averaged together.

The spectra of nanoparticle-loaded droplets, nanoparticle-free droplets and nanoparticles were measured with a spectrophotometer UV-3101 (Shimadzu, Kyoto, Japan). Samples were diluted in a 1.5 mL cuvette and the absorption spectrum was measured.

2.4 Optical vaporization

Optical droplet vaporization was studied using the experimental set-up shown in Fig. 2. The set-up consists of a dark field microscope incorporating two additional light sources; a continuous wave (CW) laser operating at 488 nm and a pulsed laser operating at 532 nm. A variable Q-switched pulsed laser with a 0.5 ns pulse width was used to induce droplet vaporization. The beam diameters of the CW and pulsed laser incident on the back of the objective were controlled to achieve 1/e beam waists of 20 μm and 15 μm, respectively, at the focal plane. The pulsed laser repetition rate was controlled with a function generator. A computer actuated attenuator was used to adjust the pulse energy such that the fluence at the sample ranged from 5 - 150 mJ/cm^2. The dynamic response of the droplets during vaporization was monitored using forward light scattering of the CW laser probe. This probe was also used to detect the dynamic response of microbubbles to pulsed laser illumination post-vaporization. The transmitted light was collected with a lens (focal length = 20 mm) and sent through an optical bandpass filter (488 nm +/– 10 nm) to a broadband photodiode. The photodiode output was sent through a 40 dB pre-amplifier and recorded on an oscilloscope.

#225025 - $15.00 USD Received 15 Oct 2014; revised 20 Nov 2014; accepted 21 Nov 2014; published 26 Nov 2014
(C) 2014 OSA

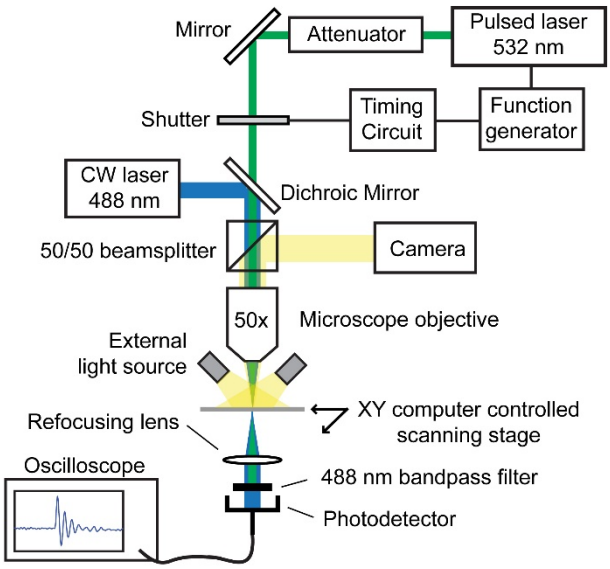

Fig. 2. Experimental setup used to study optical droplet vaporization.

In order to measure single droplet vaporization events, the laser was operated at a 10 Hz and individual pulses selected using a computer controlled shutter. In all other experiments, the shutter remained open and the laser repetition rate was set to 1 kHz. The droplets were housed between a microscope slide and coverslip, and the edges of the coverslip sealed with vacuum grease. This arrangement was then placed on an x-y computer controlled scanning stage at the focal plane of the microscope.

3. Results and discussion

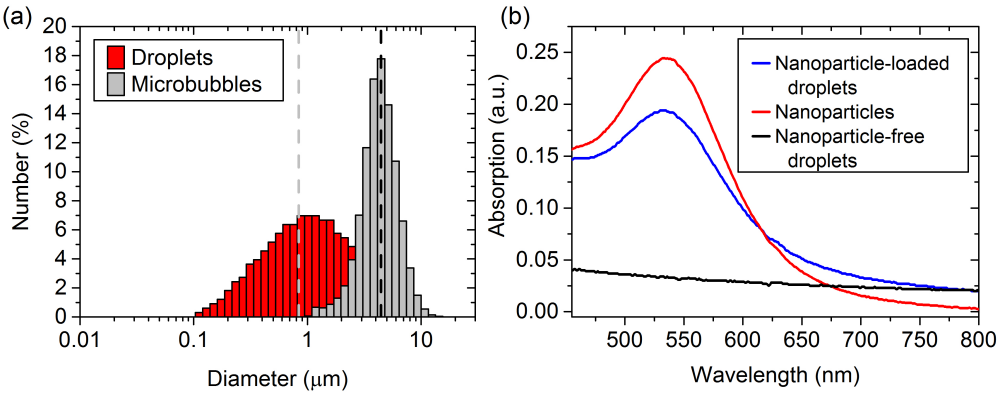

Fig. 3. (a) Size distribution of nanoparticle-coated microbubbles and the droplets produced after condensation of the microbubbles. (b) Absorption spectra comparing nanoparticles, nanoparticle-coated droplets and nanoparticle-free droplets.

A histogram of the size distribution of nanoparticle-templated C_4F_{10} microbubbles before condensation and the droplets produced after condensation is shown in Fig. 3(a). The median diameter of the microbubbles (shown as the dark, dashed vertical line) was 4.45 μm. Assuming conservation of mass, microbubbles with a core of C_4F_{10} would condense to droplets with a diameter 5.3 times smaller than the initial microbubble. The lighter, dashed vertical line depicts the theoretical median diameter of the droplets assuming a 5.3 fold

#225025 - $15.00 USD Received 15 Oct 2014; revised 20 Nov 2014; accepted 21 Nov 2014; published 26 Nov 2014
(C) 2014 OSA

change (0.84 μm). The measured median diameter of the droplets was 0.88 μm, close to the expected value. The absorption spectra of nanoparticle-loaded C_4F_{10} droplets, nanoparticles alone, and nanoparticle-free C_4F_{10} droplets are shown in Fig. 3(b). The nanoparticles show the expected absorption peak associated with the plasmon resonance wavelength around 535 nm. The spectrum for the nanoparticle loaded droplets is similar to that observed for the nanoparticles alone, indicating that the nanoparticle loading is preserved in the condensation process. In addition, the absence of a spectral shift provides evidence that there is little nanoparticle clumping or aggregation subsequent to condensation.

In order to investigate the dynamic response of C_4F_{10} droplets, a droplet was located within the field of view of the microscope and positioned at the center of the pulsed laser pump beam and CW probe laser. We note that due to the relatively close index of refraction match between liquid C_4F_{10} and water, droplets are generally quite difficult to locate. Nevertheless, some of the larger droplets could be identified and remained stationary during the measurements. For this experiment, the pump laser fluence was increased in steps of 2 mJ/cm^2 and at each fluence the response from the scattered probe beam was recorded. This process was then repeated until a vaporization event was observed. Figure 4(a) shows a representative result of such an experiment, where vaporization was observed at a laser fluence of 22 mJ/cm^2. The signal observed at one fluence step before vaporization (20 mJ/cm^2) is also shown in the figure. Below the optical threshold for vaporization the light level on the photodetector remained at a constant level, with any optical scattering from, for example, photothermal droplet heating below the noise level of the system. Above the vaporization threshold, the core rapidly expands and reaches a maximum diameter in approximately 1 μs. The resulting microbubble then undergoes several oscillations before reaching a steady state diameter of 7 μm. We note that the forward light scattering signal is not directly proportional to the bubble size as a vapor nuclei forms and grows into a bubble, and one must take this into account when interpreting the dynamic response. Previous experiments have shown that over the limited radius range (1-6 μm), the light scattering signal reduction at the photodetector scales with the square of bubble size. We do note that a small amount of bubble growth was observed at later times (several seconds) most likely due to gas efflux and influx of the core [26,27].

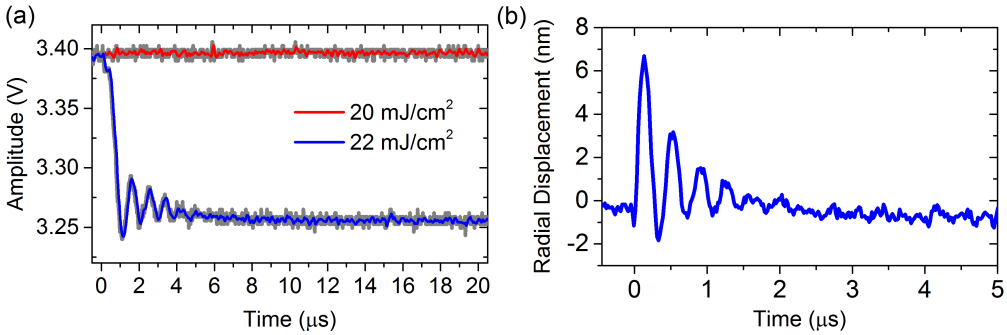

Fig. 4. (a) The response of a droplet to a single optical pulse before vaporization at 20 mJ/cm^2 and during vaporization when the pulsed laser was increased to 22 mJ/cm^2. The unfiltered response is shown as the gray line where the solid blue and red lines have been digitally filtered with a 10 MHz low-pass filter. (b) The photoacoustic response of a microbubble produced from droplet vaporization illuminated with a fluence of 15 mJ/cm^2.

We have previously shown that nanoparticle-loaded microbubble oscillations can be induced by a pulsed laser source, and that the photoacoustic response from such microbubble populations exceeds that from free nanoparticles at the same nanoparticle concentration [22,28]. The microbubbles produced post vaporization remain optically active, indicating that the nanoparticles are not purged during the explosive vaporization of the droplet core. An

#225025 - $15.00 USD Received 15 Oct 2014; revised 20 Nov 2014; accepted 21 Nov 2014; published 26 Nov 2014
(C) 2014 OSA

example of the dynamic response of a microbubble, post C_4F_{10} droplet vaporization, is shown in Fig. 4(b). Here, the vaporized bubble is positioned at the center of the pump and probe beams illuminated with a laser fluence of 15 mJ/cm^2. The fluctuation in optical power at the photodetector, averaged over 6,000 measurements, was converted to radial displacements using the previously determined conversion curve [28]. The shell elasticity can be extracted from the bubble response. Here, the bubble diameter was 3.56 μm and the measured resonant frequency was 2.67 MHz, giving a shell elasticity of 0.41 N/m. The shell elasticity is within the range, but on the lower side, of previously reported values [28]. Based on the measured bubble response one can conclude that the vaporized droplet retains a lipid shell with attached nanoparticles. We note a total of 18 microbubbles were interrogated post vaporization and all of them were found to be optically active.

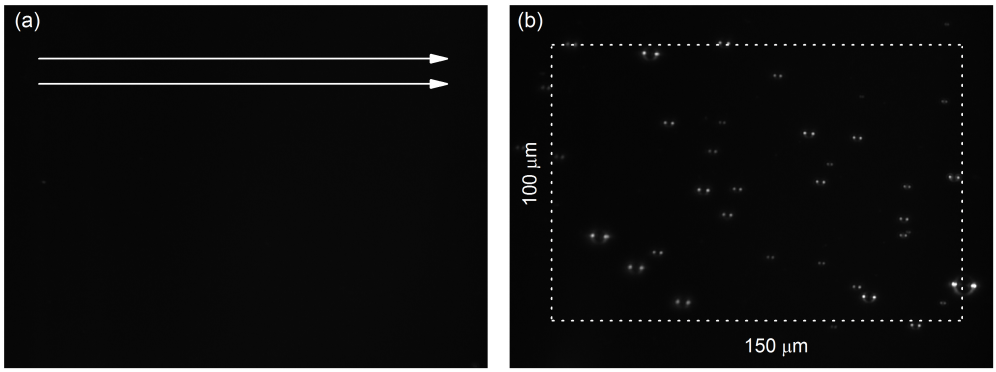

Fig. 5. (a) The dark field microscopy image captured after scanning the pulsed laser at a fluence of 10 mJ/cm^2, the white lines with arrows indicate the scanning direction. (b) The resulting vaporized bubbles with dashed lines outlining the scanned area which is 100 μm in the vertical direction and 150 μm in the horizontal direction. The pulsed laser fluence was 50mJ/cm^2.

As mentioned earlier, it is somewhat difficult to identify droplets (particularly sub-micron droplets) within the field of view of the microscope. Rather than identify droplet position *a priori*, threshold fluence measurements were made by illuminating an area of the sample and determining the number of vaporization events that occurred at a given fluence. Here the pump laser repetition rate was set at 1 kHz, and the sample was first raster scanned over a fixed area at a low (sub threshold) laser fluence. The laser fluence was then increased and the process repeated. At each laser fluence, the number of new bubbles appearing in the scan area was determined based on the acquired dark field microscopy image. The process is illustrated in Fig. 5, where Fig. 5(a) shows the optical image after raster scanning a sample of C_4F_{10} droplets at a laser fluence of 10 mJ/cm^2, where no vaporization events (microbubbles) are observed. Figure 5(b) shows the same area after a scanning with a laser fluence of 50 mJ/cm^2. Here, the majority of the droplets within the scan area have been vaporized to produce the observed microbubbles. The image also provides a means of sizing the microbubbles. This process is repeated over multiple scan areas in order to determine the variation in the threshold fluence for droplet vaporization within droplets with a given PFC core.

The threshold fluences for vaporization of C_3F_8, C_4F_{10} and C_5F_{12} droplets was determined using the raster scan approach. Scans were performed at a given fluence step (ΔF) and the number of new vaporization events (N_f) was found. Frequency density histograms were then constructed by dividing N_f by the total number of observed vaporization events and normalizing this by ΔF, and the results are shown in Fig. 6(a)-6(c). The solid lines show the fit to a log-normal probability density function, from which a 50% threshold for droplet vaporization can be determined. C_3F_8 droplets had a 50% threshold fluence of 10.6 ± 5.1 mJ/cm^2 (mean ± standard deviation), C_4F_{10} droplets had a threshold of 26.1 ± 21.7 mJ/cm^2,

#225025 - $15.00 USD Received 15 Oct 2014; revised 20 Nov 2014; accepted 21 Nov 2014; published 26 Nov 2014
(C) 2014 OSA

and C_5F_{12} droplets at 97.4 mJ/cm^2 ± 20 mJ/cm^2. As might be expected, the lower boiling point PFCs have lower threshold fluences required for vaporization. Perhaps more relevant when considering homogeneous bubble nucleation within the droplet core, are the core material critical temperatures: 345.1 K for C_3F_8, 386.4 K for C_4F_{10} and 422 K for C_5F_{12}. Again the vaporization scales with critical temperature, with a change in droplet core from C_5F_{12} to C_3F_8 giving more than a nine fold decrease in threshold fluence. While the results here are for gold nanospheres illuminated at a wavelength of 532 nm, we expect the same trend for any nanoparticle type and illumination wavelength so long as the droplet vaporization is triggered by linear photothermal heating processes. In particular, a low boiling point droplet arrayed with NIR absorbing nanorods may allow for droplet vaporization at significant depth in biological tissue. We also note that after optical vaporization of droplets with a C_3F_8 core the size distribution of vaporized bubbles was shifted to smaller diameters with respect to the initial microbubbles used for condensation. We hypothesize that this is due to increased dissolution of the gas core during condensation due to the increased solubility of the gas.

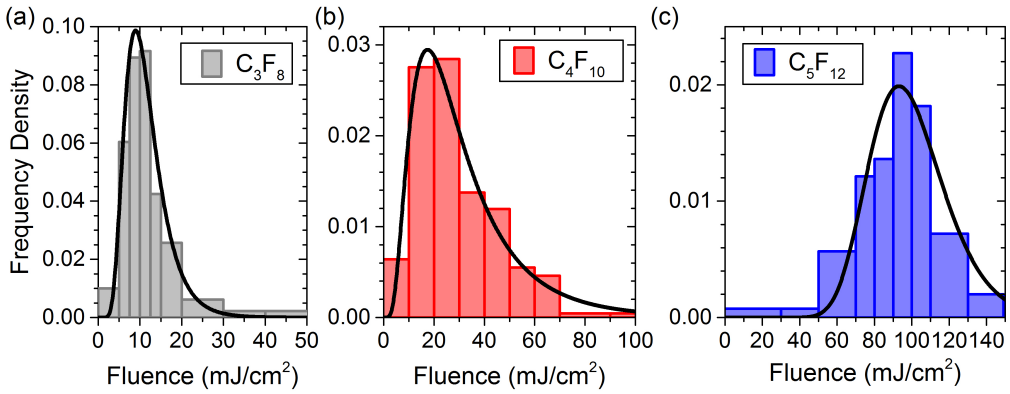

Fig. 6. Frequency density histograms of droplet vaporization with increasing fluence for three different cores (a) C_3F_8, (b) C_4F_{10} and (c) C_5F_{12}.

Droplet vaporization is initiated when a nucleus of critical size is formed within the droplet and subsequently expands into a bubble. While the spatial distribution of nanoparticles on the droplet after microbubble condensation is unknown, it is expected that they are concentrated on the periphery and lead to rapid preferential heating near the PFC/water interface. Here we assume homogeneous nucleation occurs in the PFC core at the superheat limit of approximately 90% of the critical temperature. The 50% threshold fluence plotted against 90% of the critical temperature for the three core materials is shown in Fig. 7(a). The dotted line shows a linear fit to the data with the intercept fixed at ambient temperature (298 K). The slope of this line (0.91 K/(mJ/cm^2)) gives a measure of the heating efficiency of the nanoparticle construct. This allows one to quantify the effectiveness of the light absorbing species in converting incident light into droplet core heating. The heating efficiency may be increased, and fluence threshold reduced, by using nanoparticles with larger absorption cross section or incorporating a different loading scheme.

The heating of a 5 nm gold nanoparticle immersed in water subject to a 0.5 ns laser pulse at wavelength of 532 nm was calculated [29]. The absorption efficiency of the nanoparticle, determined from Mie theory, is 0.29. Figure 7(b) shows the heating efficiency (maximum temperature rise normalized by the excitation laser fluence) as a function of distance from the gold-liquid interface. The horizontal dashed line shows the heating efficiency found from the linear fit of the data in Fig. 7(a), and the two curves intersect at a distance of 4.32 nm from the gold-water interface. The nanoparticles are attached to the droplet shell on the distal end of the PEG which is in a brush configuration. The length of the PEG brush layer can be estimated from self-consistent field theory [30,31]. Assuming the monomer length of the PEG

#225025 - $15.00 USD Received 15 Oct 2014; revised 20 Nov 2014; accepted 21 Nov 2014; published 26 Nov 2014
(C) 2014 OSA

as 0.35 nm and a lipid head group area of 0.44 nm^2 the length of the brush layer is estimated to be 4.40 nm, which is close to the predicted thermal length.

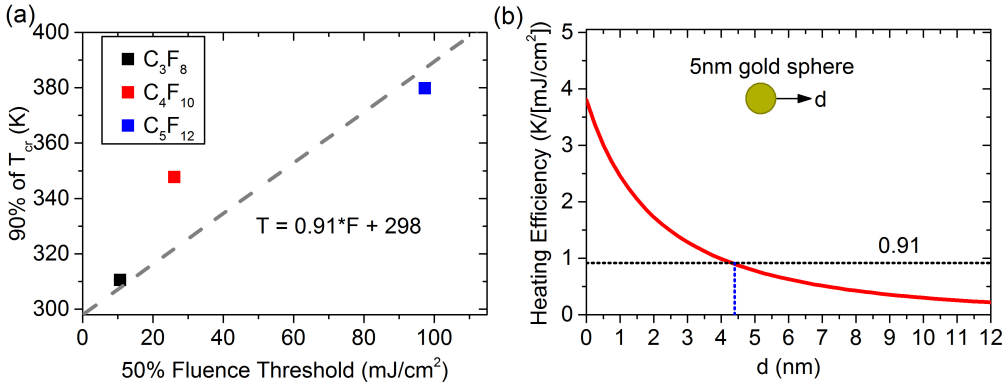

Fig. 7. (a) The fluence to vaporize 50% of the droplets plotted against 90% of critical temperature. The gray dashed line is a linear fit to the data with a y-intercept set to 298 K. (b) The heating efficiency of a 5nm gold sphere surrounded by water is plotted as a function of the distance from gold-liquid interface. The black dotted line is the estimated heating efficiency from the experiments and the blue dotted line is the estimated length of the PEG brush layer.

This simple model also provides some insight to the broad range of threshold fluences within the droplet population observed for all three PFCs. The maximum temperature rise produced by pulsed laser heating is highly dependent on distance from the nanoparticle surface. For example, a 25% higher peak temperature occurs at a distance of 3.5 nm compared to 4.5 nm. The fluence at which the core temperature reaches the nucleation threshold is thus a strong function of the spatial configuration of the nanoparticles with respect to the core and variations in PEG coverage and nanoparticle loading between droplets may be responsible for the distribution in threshold fluences. We also note that overlapping thermal fields between closely spaced nanoparticles as well as nanoparticle clustering also can have a strong influence on the local temperature rise [32,33].

Bubble size distributions have also been determined after laser vaporization and compared to those prior to condensation. A histogram of the size distributions for C_4F_{10} bubbles is shown in Fig. 8(a). The median diameters of the bubbles before condensation and after vaporization were 3.6 µm and 3.4 µm, respectively. In previous work, a small amount of gas dissolution from the microbubble was observed during the condensation process [23]. This would result in a loss of core mass leading to a slightly smaller vaporized bubble. Nevertheless, the size distribution is well-maintained through the condensation and laser induced vaporization process; an important feature of the agents for dual mode imaging applications where strong scattering from the vaporized droplet population is desired [34,35].

In order to investigate the effect of microbubble size on the vaporization threshold, a droplet population was scanned under a given laser fluence and the number and size of new microbubbles formed were recorded. The laser fluence was then increased and the process repeated. The results of this experiment are shown in Fig. 8(b)-8(d). Figure 8(b) shows the size distribution of microbubbles with fluence thresholds between 0 and 14 mJ/cm^2, while Fig. 8(c) and Fig. 8(d) show the distributions with thresholds of 14-30 mJ/cm^2 and 30-60 mJ/cm^2, respectively. We note that the vaporized droplet size distribution can be inferred from the microbubble distribution by dividing by a factor of 5.3. Interestingly, the size distribution of microbubbles produced by droplet vaporization at low laser fluence is similar to that produced at high laser fluence. In other words, we find a broad distribution of fluence thresholds for droplets of a given size and no indication of larger droplets having lower fluence thresholds.

#225025 - $15.00 USD Received 15 Oct 2014; revised 20 Nov 2014; accepted 21 Nov 2014; published 26 Nov 2014
(C) 2014 OSA

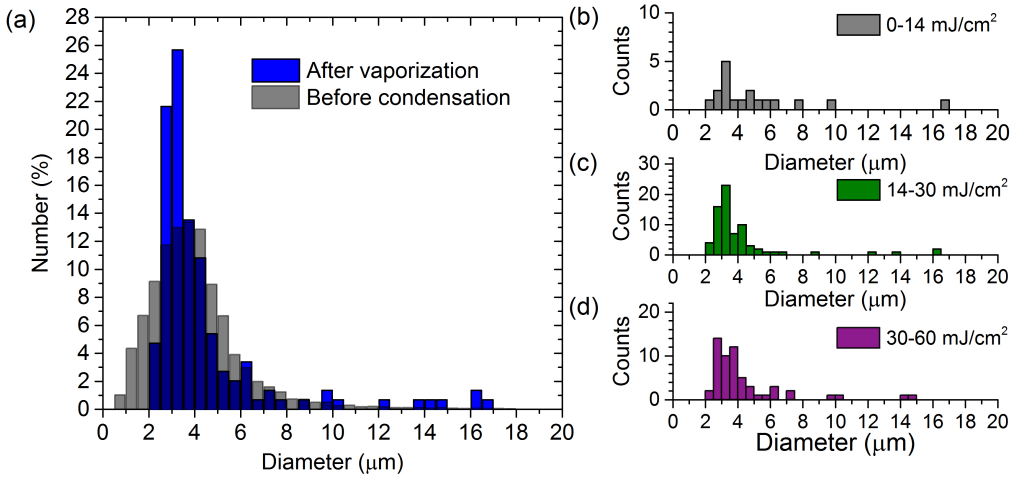

Fig. 8. (a) Comparison of the size distribution of C_4F_{10} bubbles prior to condensation and the bubbles produced from droplet vaporization. (b-d) Size distributions of vaporized C_4F_{10} bubbles with fluence thresholds of (b) 0-14, (c) 14-30, and (d) 30-60 mJ/cm^2.

It is expected that the primary influence of size on vaporization may stem from the surface tension at the liquid-liquid interface, causing the pressure in the droplet core to increase with decreasing droplet radius. The increased pressure in the droplet core may require a larger vapor embryo (critical nucleus) to trigger droplet vaporization and thus higher laser fluence. The droplets used in these experiments are encapsulated with a lipid monolayer, and the surface tension is influenced by the level of compression. Prediction of droplet size effects on threshold fluence is complicated by the fact that the surface tension is not known. Referring back to Fig. 8, if the effects of surface tension are large, one would expect the lower fluences to primarily trigger vaporization events in larger droplets producing, in turn, larger microbubbles. The fact that this is not observed leads us to believe that the broad distribution in threshold fluences (Fig. 6) may be associated with the distribution of nanoparticles around the droplet core and that droplet size and surface tension may play a secondary role.

4. Conclusions

In conclusion, we have demonstrated the ability to control the optical vaporization threshold through manipulation of the core material. We utilized a condensation technique for droplet fabrication and were able to produce droplets in a metastable, superheated state. The lowest threshold fluence for vaporization was 10.6 mJ/cm^2 for a C_3F_8 core. This was 9 times lower than C_5F_{12}, a commonly used core material for optical and acoustic droplet vaporization. The vaporization threshold fluence could be lowered further by utilizing, for example, a nanoparticle shell that offers more efficient heating, such as nanorods which have additional benefits of absorbing in the NIR. In addition, application of ultrasound in combination with pulsed laser illumination could further reduce the optical vaporization threshold [36]. The threshold fluence for droplet vaporization was found to scale with critical temperature of the core material. Previous research has demonstrated that a range of vaporization thresholds can be achieved by utilizing a mixture of two different core materials [18,37]. This would provide an additional avenue to fine tune PFC droplets as optical probes with powerful applications in imaging or therapy.

#225025 - $15.00 USD Received 15 Oct 2014; revised 20 Nov 2014; accepted 21 Nov 2014; published 26 Nov 2014
(C) 2014 OSA